Nanotechnology **19** (2008) 375701 (4pp) doi:10.1088/0957-4484/19/37/375701

Surface enhanced Raman scattering of silver sensitized cobalt nanoparticles in metal–dielectric nanocomposites

J Margueritat[1,2,7], J Gonzalo[1], C N Afonso[1], U Hörmann[3], G Van Tendeloo[3], A Mlayah[2], D B Murray[4], L Saviot[5], Y Zhou[6], M H Hong[6] and B S Luk'yanchuk[6]

[1] Laser Processing Group, Instituto de Optica, CSIC, Serrano 121, 28006 Madrid, Spain
[2] Centre d'Elaboration de Matériaux et d'Etudes Structurales CNRS/Université Paul Sabatier, 29, rue Jeanne Marvig, BP 94347, 31055 Toulouse Cedex 4, France
[3] EMAT, University of Antwerp, Groenenborgerlaan 171, B-2020 Antwerp, Belgium
[4] Mathematics, Statistics and Physics Unit, University of British Columbia Okanagan, 3333 University Way, Kelowna, BC, V1V 1V7, Canada
[5] Institut Carnot de Bourgogne, UMR CNRS 5209, Université de Bourgogne, 9 Avenue Alain Savary, BP 47870, 21078 Dijon Cedex, France
[6] Data Storage Institute, Agency for Science, Technology and Research, DSI Building, 5 Engineering Drive 1, Singapore 117608, Republic of Singapore

E-mail: j.margueritat@io.cfmac.csic.es

Received 19 May 2008, in final form 8 July 2008
Published 1 August 2008
Online at stacks.iop.org/Nano/19/375701

Abstract
We report the preparation of a new type of nanocomposite containing cobalt and silver nanoparticles organized in parallel layers with a well controlled separation. This arrangement allows the observation of an enhanced low-frequency Raman signal at the vibration frequency of cobalt nanoparticles excited through the surface plasmons of silver nanoparticles. Numerical simulations of the electric field confirm the emergence of hot spots when the separation between silver and cobalt nanoparticles is small enough.

(Some figures in this article are in colour only in the electronic version)

1. Introduction

Nanocomposites made from metal nanoparticles (NPs) in dielectrics are the focus of a major research effort driven by their potential applications in plasmonics [1], data processing [2, 3] or bioimaging [4–7]. In particular, the design of efficient and reproducible structures for controlled enhanced Raman scattering allowing the increase of the otherwise small Raman signal by many orders of magnitude is a current challenge.

In the last few years it has been demonstrated that collective optical, magnetic and transport properties can result from self-organization of NPs. In addition, systems containing either magnetic or noble metal NPs continue to generate great interest due to the possibility of achieving large electromagnetic field enhancement via surface plasmon resonance (SPR) [8, 9]. This makes the production and study of nanostructured and self-organized materials containing different types of metal NPs particularly attractive.

In this work we report on the control of the interaction between Ag and Co NPs when combined in a single system. Using alternate pulsed laser deposition (PLD) [10, 11] we succeeded in producing samples in which the NPs are organized in parallel layers. By varying the average separation between Co and Ag NP layers in the range 4–8 nm, the degree of exposure of Co NPs to the near field of Ag NPs excited by light can effectively be modified. The results presented show that the inelastic light scattering by the confined acoustic vibration of Co NPs can be excited through the SPR of Ag NPs when the separation between Co and Ag NPs becomes shorter than a critical value.

[7] Author to whom any correspondence should be addressed.

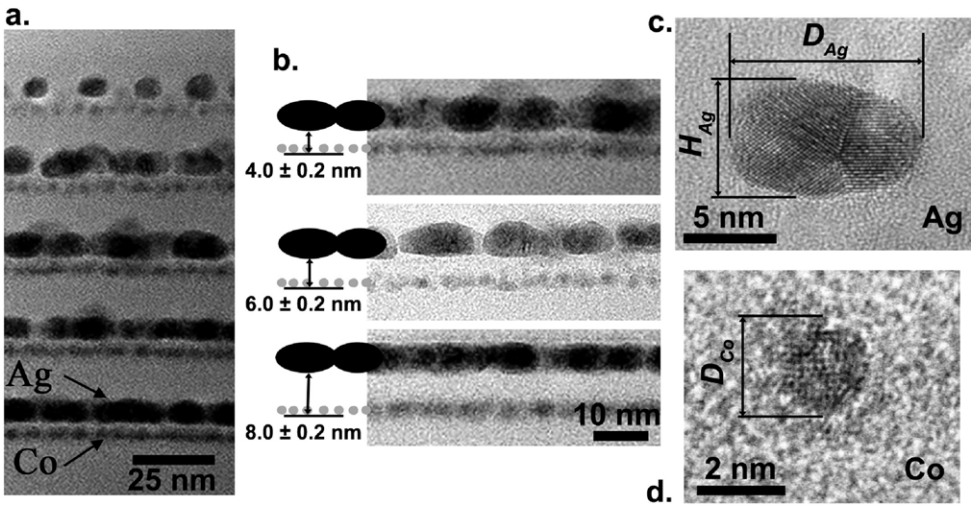

Figure 1. Cross section TEM images of samples containing Co–Ag bilayers embedded in a-Al_2O_3: (a) overall view of a sample containing five Co–Ag bilayers spaced $X = 4.0 \pm 0.2$ nm; (b) from top to bottom, magnified images of Co–Ag bilayers for $X = 4.0 \pm 0.2$, 6.0 ± 0.2, and 8 ± 0.2 nm. High-resolution TEM images of (c) a Ag oblate NP and (d) Co NPs.

2. Experimental details

The samples were produced by alternate pulsed laser deposition (PLD) using an ArF excimer laser (pulse duration 20 ns, energy density 1.9 J cm^{-2}). The beam was alternately focused on the surface of high-purity Al_2O_3, Ag and Co rotating targets. The samples were produced in vacuum ($<10^{-7}$ mbar) on rotating Si substrates held at room temperature and placed 32 mm away from the target surface. They consist of five pairs of layers of Co and Ag NPs spaced by amorphous Al_2O_3 (a-Al_2O_3). The spacing between layers has been controlled through the number of laser pulses in the Al_2O_3 target. The deposition rates of Ag, Co, and a-Al_2O_3 were selected from earlier works [10–12] to produce spherical Co NPs and oblate Ag NPs. Reference samples containing five single layers of Co or Ag NPs were also produced.

The morphology and structure of the films were studied by conventional and high-resolution transmission electron microscopy (TEM) in a JEOL 4000EX operating at 400 kV. The cross-sectional samples were prepared by standard mechanical polishing followed by ion milling. Low-frequency Raman spectra were recorded using a T800 Coderg spectrometer and excited with 488 nm line of an Ar^+ laser. The incident beam was p-polarized, and the angle of incidence was 60° with respect to the normal to the sample surface. The scattered light was detected along the normal to the surface.

3. Results

Figure 1(a) shows a cross section TEM image of a sample consisting of five NP pairs of layers embedded in a-Al_2O_3. Each pair consists of a Co NP layer and a Ag NP layer, referred to as a Co–Ag bilayer. The average in-depth spacing between Co and Ag NP layers is $X = 4.0 \pm 0.2$, 6.0 ± 0.2, and 8.0 ± 0.2 nm within each bilayer for the different samples produced (figure 1(b)), while the separation between consecutive Co–Ag bilayers is 25 nm in all cases (figure 1(a)). The Ag NPs are oblate and have an average height $H_{Ag} = 6.0 \pm 0.5$ nm and an average diameter $D_{Ag} = 10 \pm 2$ nm (figure 1(c)). The Co NPs are spherical and have an average diameter $D_{Co} = 2.7 \pm 0.4$ nm (figure 1(d)). Lattice fringes are observed in figures 1(c) and (d) indicating the crystalline structure of Ag and Co NPs, respectively. In addition, it is seen that the Co NPs are single crystals while the Ag NPs are polycrystalline, since regions having different orientations are clearly observed in figure 1(c).

The low-frequency Raman spectra are presented in figure 2. The featureless spectrum corresponds to the reference sample containing only Co NPs. Instead, the reference sample containing only oblate Ag NPs presents a band at ~ 8 cm^{-1} which corresponds to the expected acoustic vibration mode of the Ag oblate NPs [12]. The Raman spectra of Co–Ag NP bilayers that are also presented in figure 2 for different in-depth vertical spacing, X, clearly show two bands for $X = 4$ and 6 nm. The low-frequency band at 8 cm^{-1} is due to the Ag NPs [12] while the broader band at ~ 27 cm^{-1} is not observed in samples containing either Ag or Co NPs only. This band also appears as a shoulder on the high-energy tail of the Raman signal due to the Ag NPs for $X = 8$ nm.

4. Discussion

The vibration frequencies of a free homogeneous isotropic elastic sphere are quantized and the vibration modes are characterized by their nature (spheroidal or torsional) and three quantum numbers n, l and m, where n labels modes in increasing order of energy and l and m are spherical harmonic integers [13]. It has been shown that only the pure radial (n, $l = 0$) and quadrupolar (n, $l = 2$) spheroidal vibration modes couple to the dipolar surface plasmons and are therefore responsible for the inelastic light scattering [14, 15]. Among them, the quadrupolar modes (n, $l = 2$) provide the dominant contribution to the low-frequency Raman scattering as observed experimentally.

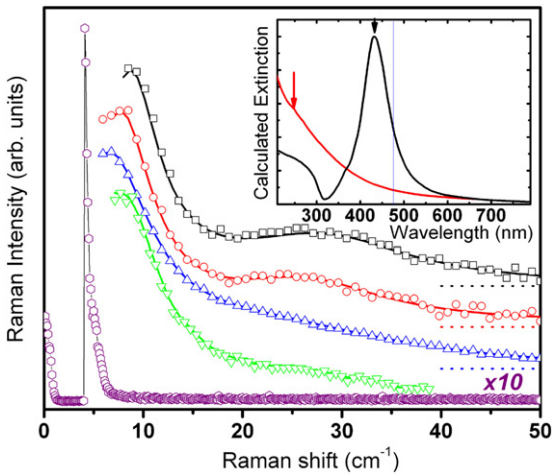

Figure 2. Stokes Raman spectra for reference samples containing only (⬡) spherical Co NPs or (▽) oblate Ag NPs, and samples containing Co–Ag bilayers with in-depth spacing (□) $X = 4.0 \pm 0.2$ nm, (○) $X = 6.0 \pm 0.2$ nm, and (△) $X = 8.0 \pm 0.2$ nm. The solid lines are guides for the eyes. The spectra were shifted vertically and normalized so that the intensity of the first peak is constant for clarity. The dotted lines represent the level 0 for each curve. The inset shows the calculated extinction spectra of (grey (red) curve) spherical Co NPs and (black curve) oblate Ag NPs embedded in a-Al_2O_3 according to Mie theory. The vertical (blue) line in the inset indicates the Raman excitation wavelength (488 nm).

The results presented in figure 2 show a clear difference between the Raman spectra of the reference samples containing either Co or Ag NPs. The spectrum of the sample containing only Co NPs is featureless; it shows no evidence for scattering by acoustic vibration modes. According to Mie's theory the SPR occurs at 250 nm; this is far away from the excitation wavelength (488 nm) used in this work, and therefore the observation of light scattering by Co NP acoustic vibrations cannot benefit from the SPR [16, 17]. Instead, the sample containing only oblate Ag NPs is excited close to their SPR and the Raman scattering by confined acoustic vibrations is observed around 8 cm^{-1}. Therefore, these results suggest that Raman scattering from Co NPs is not expected from samples consisting of Co–Ag bilayers while that due to Ag NPs should be observable. This is indeed verified in the Raman spectra of Co–Ag bilayers shown in figure 2. The intense band around 8 cm^{-1} corresponds to scattering by confined acoustic vibrations of Ag NPs, whereas a new broad band around 27 cm^{-1} appears for $X = 4$ and 6 nm. For $X = 8$ nm, the presence of this band is responsible for the high-frequency asymmetry of the main peak located at 8 cm^{-1}. In order to determine its origin we have calculated the acoustic vibration modes of each type of NP. Since crystalline Ag and Co NPs show no preferential orientation, we considered isotropic elasticity using the following 3D averaged longitudinal (v_L) and transverse (v_T) sound velocities: $v_L(\text{Co}) = 6050$ m s^{-1}, $v_T(\text{Co}) = 2886$ m s^{-1}, $v_L(\text{Ag}) = 3750$ m s^{-1} and $v_T(\text{Ag}) = 1740$ m s^{-1}. Assuming that Co NPs embedded in a-Al_2O_3 behave as free-standing NPs, their vibration frequencies can be calculated from Lamb's model. For 3 nm diameter spherical Co NPs, we obtain $\omega_{n=1,l=2} = 27$ cm^{-1}, which is in good agreement with the experimental value of the high-frequency band observed in the Raman spectra of the Co–Ag bilayers (figure 2).

Moreover, the vibration eigenfrequencies (and associated displacements) of the NPs have been calculated in the frame of the continuum elastic approximation using the 'xyz algorithm' also known as resonant ultrasound (RUS) introduced by Visscher *et al* [18]. This numerical method allows modeling the acoustic vibrations of non-spherical and elastically anisotropic objects. The frequencies have been double-checked by the finite element mesh sequence (FEMS) introduced in a previous work [19, 20]. The capability of this method to determine the acoustic vibrations irrespective of the shape of the NPs is particularly relevant for the case of our oblate Ag NPs. In the case of Ag NPs, we find that the five-fold degenerate quadrupolar vibration modes ($n = 1$, $l = 2$) split into three different frequencies when the aspect ratio, $H_{\text{Ag}}/D_{\text{Ag}}$, becomes smaller than 1, as in our case [12, 19, 20]. These frequencies are associated with spheroid-like modes, 5.1 cm^{-1} (two-fold degenerate), 6.3 cm^{-1} (non-degenerate) and 6.4 cm^{-1} (two-fold degenerate). If we take into account the effect of the matrix [11], these frequencies are in agreement with the measured Raman band frequency at 8 cm^{-1}. Moreover, the frequency of the radial mode ($n = 1$, $l = 0$) of oblate Ag NPs is found at 15.0 cm^{-1}, and thus, it cannot be responsible for the band observed at 27 cm^{-1}. Finally, we have also performed RUS simulations of a free-standing spherical Co NP. HRTEM images revealed that the Co NPs are single domain and therefore their elasticity is not isotropic. As a result, the five-fold degenerate spheroidal ($n = 1$, $l = 2$) isotropic mode at 27 cm^{-1} splits into three frequencies at 26.7 (degeneracy 2), 27.4 (degeneracy 2) and 35.1 cm^{-1} (degeneracy 1) due to elastic anisotropy (see [23], which contains the relevant elastic constants for cobalt). This is in good agreement with Lamb's theory and very close to the high-frequency band observed in the Raman spectra for the Co–Ag bilayers (figure 2).

The vibration dynamics calculations suggest that the Raman band at ≈27 cm^{-1} corresponds to confined acoustic vibrations of the Co NPs even though the excitation wavelength is far from their SPR. The coupling mechanism between the confined acoustic vibrations and the surface plasmons is needed in order to understand how these acoustic vibrations are optically excited and how they scatter light. Moreover, figure 2 shows that the vibration peaks are slightly shifted, which is probably due to the modification of the efficiency of the coupling mechanism as the separation is changed. However, this point is still under investigation. According to reference [16], the Raman scattering by confined acoustic vibrations is due to the modulation of the surface polarization charges by the NP motion.

We have thus investigated the distribution of the surrounding electric field generated by the Ag surface plasmon as a function of the spacing, X, between the Ag and Co NP layers. The calculations were carried out with finite difference time domain CST® Microwave Studio software. We have assumed that the Ag and Co NPs have respectively perfect

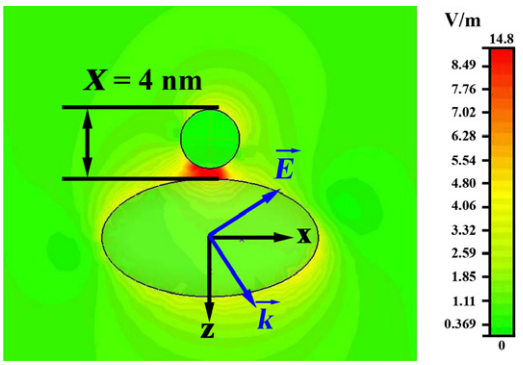

Figure 3. False color distribution of the electric field generated in the vicinity of an oblate Ag NP with a neighbor Co NP separated $X = 4.0 \pm 0.2$ nm.

oblate spheroidal and spherical shapes. The excitation source was a normalized p-polarized plane monochromatic wave at 488 nm with an angle of incidence of 60° with respect to the normal to the sample surface. The dimensions of the Ag and Co NPs were kept constant and equal to those experimentally determined, while the distance X was varied smoothly from 3 to 16 nm. The refractive indexes used were 1.67 for the matrix [11] and $n_{\mathrm{AgNP}} = 0.13+\mathrm{i}2.81$ and $n_{\mathrm{CoNP}} = 4.68+\mathrm{i}7.17$ for Ag and Co NPs, respectively [21, 22]. As expected, the electric field at the Co NP surface is very weak (the typical dipolar pattern is calculated for $X = 12$ nm). This is because the surface plasmons of the Co NP are not excited by the incident laser beam contrary to what happens to the Ag NP (see the inset in figure 2). However, the presence of the Co NP in the near field of the Ag NP has a strong impact on the electric field distribution, as shown in figure 3 for $X = 4$ nm. A hot spot characteristic of the electric field enhancement emerges in the region between the Ag and Co NPs. Moreover, the electric field in the vicinity of the Co NP surface increases by an order of magnitude when X decreases from 12 to 4 nm. According to the electromagnetic theory of surface enhanced Raman scattering, this enhancement factor should lead to a factor $\sim 10^4$ in the Raman scattering intensity due to photon absorption and emission events. So we interpret the observation of the Raman scattering by the quadrupolar acoustic vibrations of the Co NPs as due to the modulation of the surface polarization charges located in the vicinity of the hot spot generated by the interaction between the Ag and Co NPs. This interaction and thus the enhancement of the Raman scattering vanish for separations between the Co and Ag nanoparticles larger than the spatial extension of the near field associated with the oblate silver, as observed experimentally (figure 2).

5. Conclusions

The nanodesign achieved for samples containing different types of metal NP using alternate PLD has made it possible to demonstrate the existence of interaction between surface plasmons and confined acoustic vibrations of NPs of different metals. This was achieved by embedding the Co NPs into the near field region of the Ag NPs. When exciting at the surface plasmon resonance of Ag NPs, the electric field intensity at the surface of both Ag and Co NPs is strongly enhanced for separations $\leqslant 6$ nm. This allows efficient modulation of the surface polarization charges by the confined acoustic vibrations of the Co NPs, thus explaining the observation of their Raman scattering under excitation at 488 nm, i.e. far from the surface plasmon resonance of isolated Co NPs.

Acknowledgments

This work was partially supported by MAT2005-06508-C02-01, MEC (Spain), and by EU Network HPRN-CT-2002-00328. JM acknowledges an I3P fellowship from CSIC and the European Social Fund and financial support from the CSIC for a stay in DSI (Singapore). DBM acknowledges support from NSERC.

References

[1] Homola J, Yee S S and Gauglitz G 1999 *Sensors Actuators* B **54** 3–15
[2] Maier S A, Kik P G, Atwater H A, Meltzer S, Harel E, Koel B E and Requicha A A 2003 *Nat. Mater.* **2** 229–32
[3] Barnes W L, Dereux A and Ebbesen T W 2003 *Nature* **424** 824–30
[4] Cao Y W C, Jin R and Mirkin C A 2002 *Science* **297** 1536–40
[5] Sönnichsen C, Reinhard B M, Liphardt J and Alivisatos A P 2005 *Nat. Biotechnol.* **23** 741–5
[6] Kneipp K, Wang Y, Kneipp H, Perelman L T, Itzkan I, Dasari R R and Feld M S 1997 *Phys. Rev. Lett.* **78** 1667–9
[7] Nie S and Emery S R 1997 *Science* **275** 1102–6
[8] Anderson N, Bouhelier A and Novotny L 2006 *J. Opt. A: Pure Appl. Opt.* **8** S227–33
[9] Bouhelier A, Beversluis M, Hartschuh A and Novotny L 2003 *Phys. Rev. Lett.* **90** 013903
[10] Dobrynin A N *et al* 2005 *Appl. Phys. Lett.* **87** 012501
[11] Margueritat J, Gonzalo J, Afonso C N, Mlayah A, Murray D B and Saviot L 2006 *Nano Lett.* **6** 2037–42
[12] Margueritat J, Gonzalo J, Afonso C N, Bachelier G, Mlayah A, Laarakker A S, Murray D B and Saviot L 2007 *Appl. Phys.* A **89** 369–72
[13] Lamb H 1882 *Proc. London Math. Soc.* **13** 198
[14] Fujii M, Nagareda T, Hayashi S and Yamamoto K 1991 *Phys. Rev.* B **44** 6243–8
[15] Portales H, Saviot L, Duval E, Fujii M, Hayashi S, Del Fatti N and Vallée F 2001 *J. Chem. Phys.* **115** 3444–7
[16] Bachelier G and Mlayah A 2004 *Phys. Rev.* B **69** 205408
[17] Gangopadhyay P, Ravindran T R, Nair K G M, Kalavathi S, Sundaravel B and Panigrahi B K 2007 *Appl. Phys. Lett.* **90** 063108
[18] Visscher W M, Migliori A, Bell T M and Reinert R A 1991 *J. Acoust. Soc. Am.* **90** 2154–62
[19] Saviot L, Murray D B and Marco de Lucas M C 2004 *Phys. Rev.* B **69** 113402
[20] Murray D B, Laarakker A S and Saviot L 2006 *Phys. Status Solidi* c **3** 3935–8
[21] Palik E D (ed) 1985 *Handbook of Optical Constants of Solids* (New York: Academic)
[22] Kudryavtsev V Y and Lezhnenko I V 1981 *Sov. Phys.—Solid State* **21** 249
[23] McSkimin H J 1955 *J. Appl. Phys.* **26** 406